Nanoscale

COMMUNICATION

View Article Online
View Journal

Bismuth oxide nanotubes–graphene fiber-based flexible supercapacitors†

Cite this: DOI: 10.1039/c4nr02615b

Karthikeyan Gopalsamy, Zhen Xu, Bingna Zheng, Tieqi Huang, Liang Kou, Xiaoli Zhao and Chao Gao*

Received 13th May 2014
Accepted 4th June 2014

DOI: 10.1039/c4nr02615b

www.rsc.org/nanoscale

Graphene–bismuth oxide nanotube fiber as electrode material for constituting flexible supercapacitors using a PVA/H_3PO_4 gel electrolyte is reported with a high specific capacitance (C_a) of 69.3 mF cm^{-2} (for a single electrode) and 17.3 mF cm^{-2} (for the whole device) at 0.1 mA cm^{-2}, respectively. Our approach opens the door to metal oxide–graphene hybrid fibers and high-performance flexible electronics.

Flexible and wearable energy devices, which are light in weight and easy for integration, are indispensable to deliver utmost unique power storage. Such devices enable stretching, bending, and twisting properties to be accomplished in high-energy storage applications.[1–4] Considerable attention has been addressed for the improvement of their supercapacitors performance, in terms of power density, capacitance and cyclic stability, for the increasing demand of powerful and robust energy storage devices.[5–8] In general, carbon materials, such as activated carbon, graphene, CNTs, templated carbons and carbons with heteroatoms, have been used as electrodes in supercapacitors.[9,10] Moreover, research on supercapacitors involving the use of graphene as electrodes has triggered much interest as they overcome low energy density and low rate capability problems. Apart from the conventional supercapacitors, 1D fiber supercapacitors have aroused as a promising form for macroscopic uses, attracted by its flexibility and stitchability.[11–15] Recently, CNT fiber-based supercapacitors were reported with a capacitance of 3.57 mF cm^{-2} with high energy density (92.84 mW h cm^{-3}) and power density (3.87 W cm^{-3}).[13] In another work, Wang *et al.* used CNT/CNT polyaniline (PANI) nanowire to fabricate FSCs and achieved a maximum capacitance up to 38 mF cm^{-2}.[14]

Recently, graphene fibers have been invented by wet-spinning of graphene-based liquid crystals or dispersions, and they possessed high mechanical performance, electrical conductivity, and importantly good flexibility.[16–19] The fiber form of electrodes is a new area in supercapacitors and is more advantageous compared to film or sheet-type graphene used in supercapacitors due to their lower weight and compactness in real-time electronics. These attributes of graphene fibers can justify their promising uses as flexible and wearable capacitors. However, graphene fiber-based supercapacitors (FSCs) are rarely reported, because of the recent discovery and fabrication of graphene fibers themselves. Huang *et al.* reported the first wet-spun graphene fiber-based SCs with a capacitance of 3.3 mF cm^{-2} at 0.1 mA cm^{-2}.[20] FSCs of graphene fibers made by hydrothermal methods and other approaches were also created recently with a capacitance range of 1.7–12.4 mF cm^{-2}.[21–23] For practical applications, it is necessary to further improve the capacitance of graphene-based FSCs. Strategies to improve the capacitive properties of graphene involve the addition of CNTs, electronically conductive polymers or metal oxides.[24,25] Fiber-based SCs with scalable capacitance using a two fiber-based electrode system have been demonstrated by Bae *et al.*[26] Very recently, high-performance coaxial fiber-based SCs with high specific capacitance (177 mF cm^{-2}) and high energy density (3.84 μW h cm^{-2}) were reported.[27] Another work showed the emphasis of fiber-based asymmetric SCs with increased operating voltage (0–1.6 V) and offered a total cell capacitance of 23.6 mF cm^{-2}.[28] This gives us the inspiration to achieve high-performance SCs with wet-spun graphene fibers.

Accordingly, we chose a metal oxide, *i.e.*, bismuth oxide nanotubes (Bi_2O_3 NTs), as an additional electrochemical component to enhance the capacitance of wet-spun graphene fiber-based SCs, since bismuth oxide and its nanostructures are environmentally friendly and have good electrical transport properties, which make them good candidates for making electronic devices.[29,30] Moreover, bismuth-based flat SCs have

MOE Key Laboratory of Macromolecular Synthesis and Functionalization, Department of Polymer Science and Engineering, Zhejiang University, 38 Zheda Road, Hangzhou 310027, P. R. China. E-mail: chaogao@zju.edu.cn

† Electronic supplementary information (ESI) available: Equations and characterization. SEM images of GGO, XRD and XPS of Bi_2O_3 NTs, HRTEM images and EDX Spectra of Bi_2O_3 NT5–GF, CV curves of Bi_2O_3NT5–GF, Bi_2O_3 NTs and bismuth nitrate in three-electrode system (*vs.* Ag/AgCl). CV and GCD curves of Bi_2O_3 NT1–GF and Bi_2O_3 NT3–GF. See DOI: 10.1039/c4nr02615b

shown excellent capacitance.[31–34] Herein, we report, for the first time, the wet-spinning of Bi_2O_3 NTs-loaded graphene fibers *via* a liquid crystal self-templating approach. The fibers were directly used as electrodes to connect all solid-state flexible FSCs. The highest specific capacitance achieved for Bi_2O_3 NT graphene fiber was 69.3 mF cm^{-2} at 0.1 mA cm^{-2}. Moreover, metal (oxides)–graphene fiber electrodes would be a promising alternative for flexible and high-performance SCs in modern electronics.

Bi_2O_3 NTs were synthesized by a hydrothermal process at 120 °C from the precursor of bismuth nitrate aqueous solution.[35] The resultant Bi_2O_3 NTs were characterized by XRD, XPS and TEM techniques. To get more robust graphene fibers, we used giant graphene oxide (GGO) sheets with ~0.8 nm thickness [19] as the host components due to their higher electrical conductivity and greater mechanical properties as compared with the common 0.5–2 μm GO sheets. The average lateral size of GGO was 22.4 μm and that after thermal annealing at 400 °C was found to be 21.9 μm (Fig. S1†). Apart from lateral size, giant graphene oxide sheets (GGO) have a high aspect ratio, which reduces defective edges and achieves a highly ordered alignment.[36] The GGO sheets can be well dispersed in water, and form a stable liquid crystal at a spinning concentration of 5 mg mL^{-1}, as confirmed by polarized optical microscopy (POM) (Fig. 1a). The GGO liquid crystal can be used as a template to load guest components to fabricate host–guest composite fibers by wet-spinning assembly technology.[37] Although the neat Bi_2O_3 NTs swiftly precipitated after agitation in water, they were well dispersed in the GGO aqueous liquid crystal dope, mainly due to the confining effect and amphiphilic nature of GGO sheets. Thus, the Bi_2O_3 NTs (5 wt%)–GGO dispersion still maintained a liquid crystal state (Fig. 1b); consequently, we prepared homogeneous dispersions of GGO and Bi_2O_3 NTs in different weight percentages of 1 wt%, 3 wt% and 5 wt% of NTs. Direct wet-spinning of the dispersions *via* the established wet-spinning assembly strategy[16] gave rise to continuous Bi_2O_3 NTs–GGO fibers. The prepared fibers were dried in vacuum and reduced by thermal annealing at 400 °C for 4 h under nitrogen atmosphere. The composite fibers with different weight percentages were denoted as Bi_2O_3 NT1–GF, Bi_2O_3 NT3–GF, and Bi_2O_3 NT5–GF, and used as electrodes to fabricate FSCs.

Fig. 1c–f show the SEM images of Bi_2O_3 NT5–GF with an average diameter of ~10 μm. The microstructures with ruptured cross-section were observed to possess a roughly round morphology. The regular alignment of graphene sheets along the fiber axis from the layered structure on their cross-sections and the aligned wrinkles on the surfaces were seen in the SEM images. This is similar to the structures of neat graphene fibers.[16,19] Moreover, Bi_2O_3 NTs are also identified as those connected between graphene sheets from SEM images (Fig. 1e and f). Fig. 1g shows the preparation of fibers by a wet-spinning technique, and the fibers were used to assemble FSCs in flat and bent states (Fig. 1h and i).

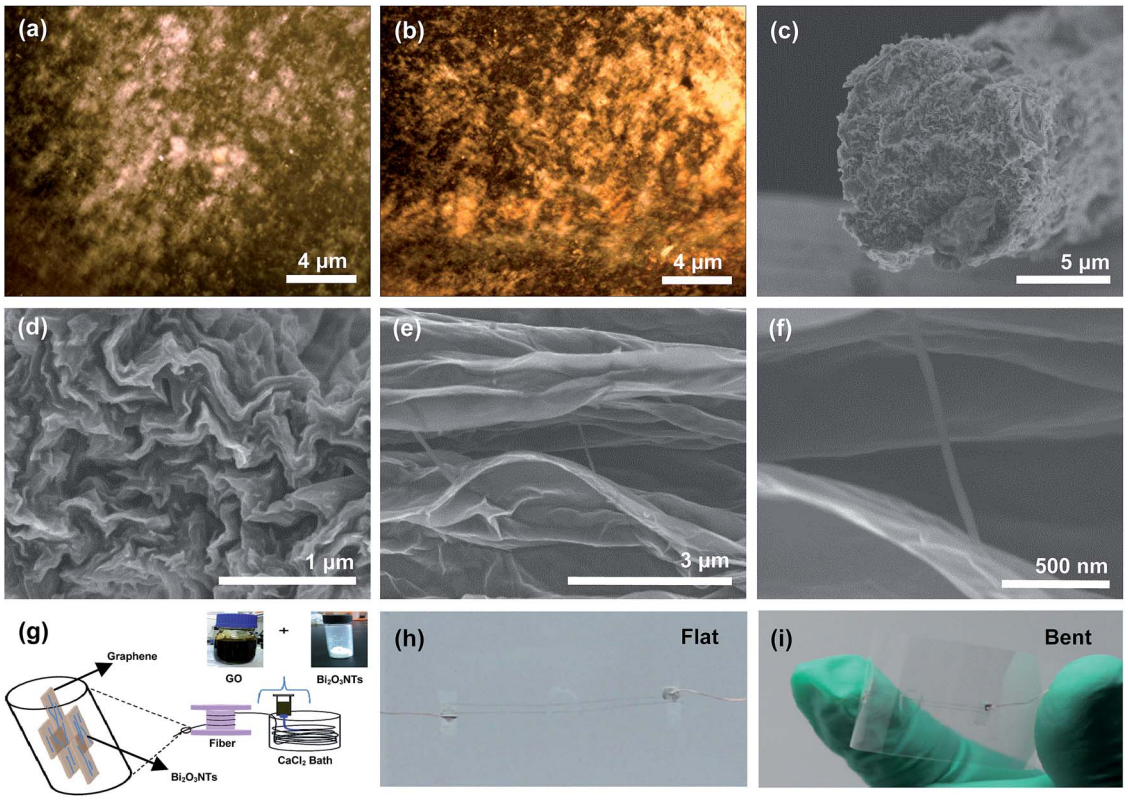

Fig. 1 POM images of dispersions of (a) GGO and (b) Bi_2O_3 NT–GGO (5 wt%). (c–f) SEM images of Bi_2O_3 NT5–GFs. (g) Wet spinning of graphene–Bi_2O_3 NT fibers. (h) and (i) Photographs of typical fiber-based micro-supercapacitor in flat and bent states.

The XRD pattern of Bi_2O_3 NTs showed that the NTs were composed of Bi_2O_3 and elemental Bi crystals (Fig. S2a†). XPS spectra of Bi_2O_3 NTs are shown in Fig. S2b and c,† where O1s and Bi4f7 peaks are centered at 537 eV and 165 eV, respectively. The corresponding TEM images revealed a tube diameter of 20–40 nm (Fig. S2d†). Fig. S2e and f† show the HRTEM images of Bi_2O_3 NTs. To clearly view the bismuth nanotubes over the graphene layers, high-resolution transmission electron microscopy (HRTEM) analysis was employed and the images are shown in Fig. S3a and b.† The presence of bismuth was further supported by the elemental analysis of energy dispersive X-ray spectra (EDX) for the sample of Bi_2O_3 NT5–GF (Fig. S3c†).

A three-electrode system with Bi_2O_3 NT5–GFs, Ag/AgCl and Pt electrodes in either 6 M KOH or 1 M H_3PO_4 electrolyte was assembled and measured (Fig. S4†). The CV curves are acquired within a small range, from −1 to 0 V, for the electrodes in 6 M KOH, and 0 to 1 V for those in 1 M H_3PO_4 electrolyte. Thus, a PVA/H_3PO_4 electrolyte was chosen to make solid FSCs in order

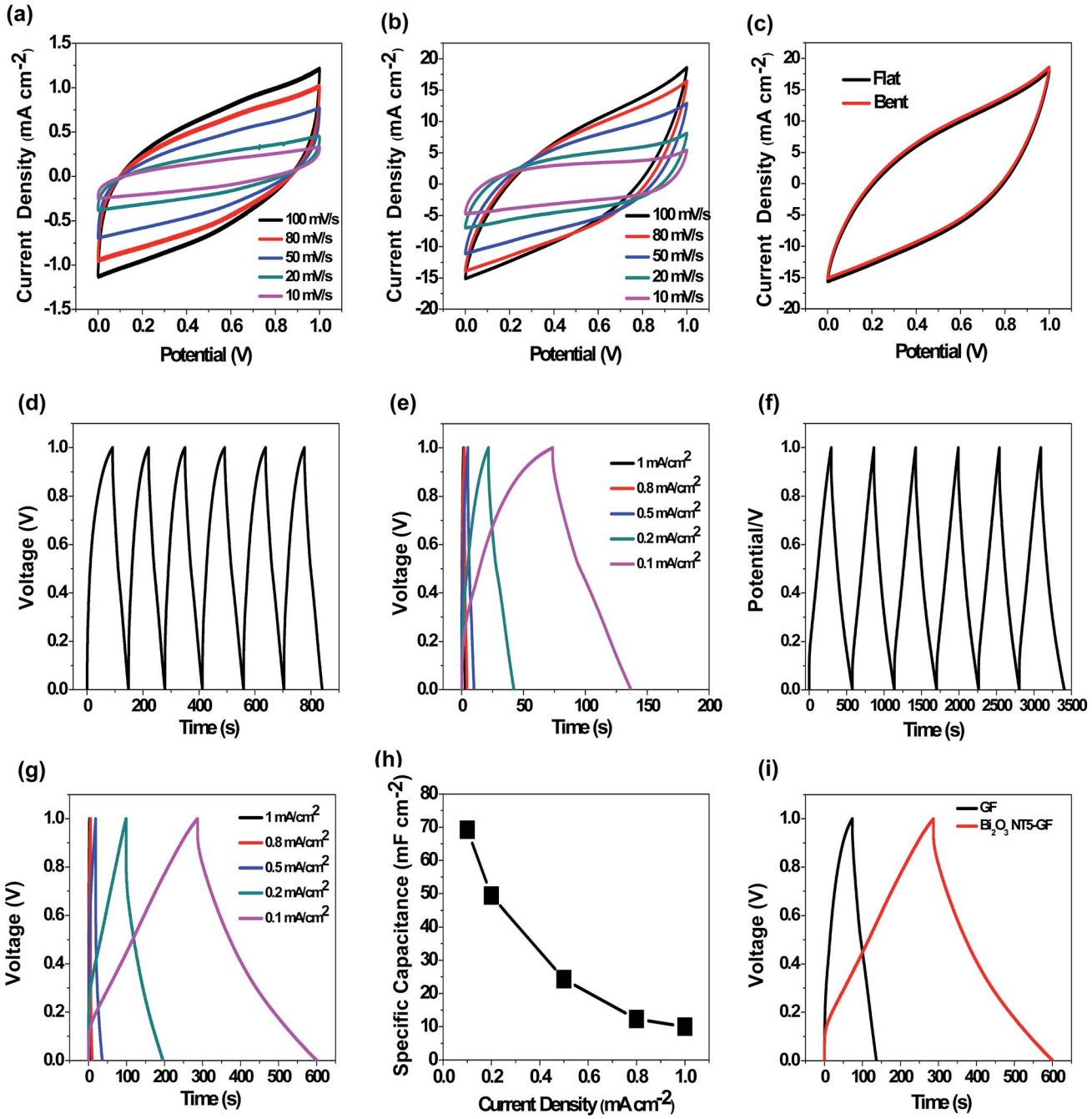

Fig. 2 (a) CV curves of GF. (b) CV curves of Bi_2O_3 NT5–GF. (c) CV curves of Bi_2O_3 NT5–GF in flat and bent states (scanning rate 100 mV s^{-1}). (d) GCD curves of GF at current density of 0.1 mA cm^{-2}. (e) GCD curves of GF at different current densities. (f) GCD curves of Bi_2O_3 NT5–GF at 0.1 mA cm^{-2}. (g) GCD curves of Bi_2O_3 NT5–GF at different current densities. (h) Specific capacitance as a function of current density for Bi_2O_3 NT5–GF. (i) GCD curves of GF and Bi_2O_3 NT5–GF at 0.1 mA cm^{-2}.

to contribute towards a stable and wide potential window. To fabricate FSCs, the fibers were directly used by parallel aligning of two fibers with ~3 mm distance in PVA/H_3PO_4 gel electrolyte.

The electrochemical performance of the as-prepared FSCs was analyzed by cyclic voltammetry (CV) at different scan rates from 10 to 100 mV s^{-1}. To evaluate the contribution of bismuth-based NTs, the neat graphene fibers-assembled supercapacitor (GFSC) was also fabricated and analyzed by CV (Fig. 2a). The CV response at different scan rates showed the increase in current response accordingly. In this case, area specific capacitance (C_a) was used to evaluate the performance of fiber-shaped supercapacitors. Based on eqn S1,† capacitance was calculated from CV data. The C_a of GF was 8.6 mF cm^{-2} at a CV scan rate of 100 mV s^{-1}, which gradually increased to 17.2 mF cm^{-2} at 10 mV s^{-1}. These values are much improved in the wet-spun thermally reduced graphene fiber supercapacitor system compared to the previous report (C_a, 1.8 mF cm^{-2} at 100 mV s^{-1} for HI reduced GFs), possibly due to the larger size of graphene sheets and thermal reduction treatment. Fig. 2b shows the CV curves of Bi_2O_3 NT5–GF at various scan rates, and the calculated C_a of the single electrode was about 19.1 mF cm^{-2} at 100 mV s^{-1} and 76.1 mF cm^{-2} at 10 mV s^{-1}. The corresponding volumetric specific capacitance (C_v) was about 35.2 F cm^{-3} at 100 mV s^{-1} and 140.1 F cm^{-3} at 10 mV s^{-1}, respectively (calculated from eqn S3†). These values are much higher than those of GF, strongly confirming the positive effect of Bi_2O_3 NTs on the electrochemical performance of graphene-based FSCs. Moreover, there was no obvious change in the capacitance for the SCs at a 45° bending angle (Fig. 2c).

To confirm the electrochemical properties, galvanostatic charge–discharge (GCD) measurements were applied at different current densities of 0.1, 0.2, 0.5, 0.8 and 1 mA cm^{-2}. The GF showed a C_a of 11.2 mF cm^{-2}, which was calculated from eqn S2,† at 0.1 mA cm^{-2} (Fig. 2d). This value is higher than that of other all-graphene core–sheath FSCs (C_a 1.2–1.7 mF cm^{-2}) by a factor of about 6.5.[23] GCD curves of GF and Bi_2O_3 NT5–GF are shown in Fig. 2d–g. The charge curves and their corresponding discharge curves were found to be symmetrical with a good linear relation of potential *versus* time; thus, they show ideal capacitive behavior, which is in good agreement with the CV curves. For Bi_2O_3 NT–GFs, the C_a was enhanced by 60% when only 1 wt% of Bi_2O_3 NTs were loaded (24 mF cm^{-2}), and enhanced by 240% by addition of 3 wt% Bi_2O_3 NTs (51 mF cm^{-2}). The CV curves and GCD curves obtained for Bi_2O_3NT1–GF and Bi_2O_3NT3–GF are shown in Fig. S5a–d.† The C_a of Bi_2O_3NT5–GF was 10 mF cm^{-2} at 1 mA cm^{-2}, and it increased to 69.3 mF cm^{-2} at 0.1 mA cm^{-2} (Fig. 2h). The specific capacitance of the device (C_D) was 17.3 mF cm^{-2} at 0.1 mA cm^{-2} as calculated from GCD curves of Bi_2O_3 NT5–GF. The C_a value is obviously higher than that of the GF at 11.2 mF cm^{-2} at 0.1 mA cm^{-2} (Fig. 2i). Moreover, the C_a value is higher than that of all-solid-state FSCs based on carbon fiber using pen ink (26.4 mF cm^{-2}),[11] CVD-derived graphene fiber (42 mF cm^{-2})[15] and CNT-PANI yarn SCs (12.0–38.0 mF cm^{-2}).[14] Electrochemical performance of various electrode materials is summarized in Table S1.† The measured specific capacitance of Bi_2O_3 NTs (0.01 mg) was found to be 0.15 mF cm^{-2} at 0.1 V s^{-1} and negligible for bismuth nitrate (Fig. S6†). Moreover, the protocol of the present work is simple and cost-effective, and it involves no binder-like polymers for dispersing Bi_2O_3–NTs in GO, which could be advantageous, since the addition of such binders reduces the capacitor performance generally.

For all the SCs, capacitance decreases as the current density increases and this could be attributed to the fact that the active ionic species are not fully utilized at high current densities. The high capacitance of Bi_2O_3 NT–GFSCs could be attributed to the nanotube structure, which is uniformly coordinated to the graphene network and thus allowed rapid charge transfer. A Ragone plot of Bi_2O_3 NT–GFs is shown in Fig. 3a, which shows that power density increases and energy density decreases when current density is increased from 0.1 to 1 mA cm^{-2}. The energy density and power density of Bi_2O_3NT5–GF were found to be 2.9 W h cm^{-3} and 33 W cm^{-3} at 0.1 mA cm^{-2}, respectively (Calculated from eqn S4 and S5†). Electrochemical impedance spectroscopy (EIS) curves of SCs of GF and Bi_2O_3NT5–GF are shown in Fig. 3b. From the impedance Nyquist plots, the equivalent series resistance (ESR) was found to be 0.6 kΩ for GFSC and 1.5 kΩ for Bi_2O_3NT5–GFSC.

As cycle durability is considered to be an imperative concern for electric double-layer capacitors, the electrochemical stability of Bi_2O_3NT5–GF for flat and at bending angle 45°, was investigated by galvanostatic charge–discharge cycling performance at a current density of 0.1 mA cm^{-2} (Fig. 3c). From observations,

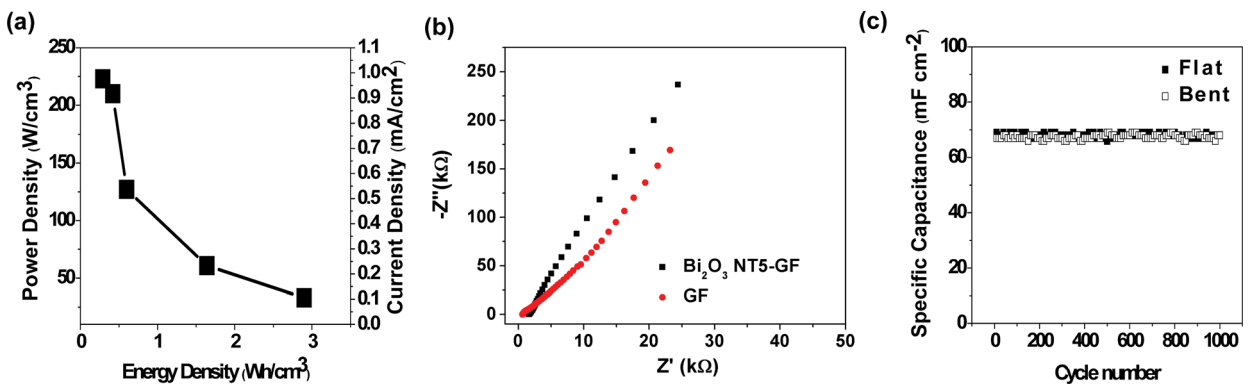

Fig. 3 (a) Ragone plot for Bi_2O_3 NT5–GF. (b) Nyquist plots for GF and Bi_2O_3 NT5–GF. (c) Cycling performance of Bi_2O_3 NT5–GF.

there was no obvious capacitance drop over 1000 cycles, indicating excellent electrochemical stability of Bi_2O_3 NT–GFSCs in both flat and bent states. The hybrid fibers have good cycle stability, and the decay of the capacitance was well below 1%. It is evident that our SCs have a unique structure in a compact manner with consistent cycling stability without significant loss of capacitance, assuring the durable nature of electrode and electrolyte.

In summary, Bi_2O_3 NT–graphene fibers were prepared by a wet-spinning process by a liquid crystal self-templating approach. This method could be readily extended to other metal oxides, opening a new avenue to metal oxide–graphene wet-spun fibers for real time applications. The as-prepared hybrid fibers were directly used to assemble FSCs. The highest specific capacitance of the GF was 11.2 mF cm^{-2} (for a single electrode) and that of robust Bi_2O_3 NT–GF was 69.3 mF cm^{-2} at 0.1 mA cm^{-2} (for a single electrode). The hybrid FSCs also demonstrate a stable cycling life of over 1000 cycles. Apart from the capacitance performance, the FSCs are flexible and compact; thus, they reduce space compared to other types like film or composite SCs. In future, developing such fiber electrode supercapacitor systems would be a new platform for designing flexible hybrid electrode materials in advanced energy storage devices.

Experimental section

Wet-spinning of Bi_2O_3 NT–graphene fibers

Bi_2O_3 NT–GGO homogeneous suspension was obtained by mixing the appropriate amount of Bi_2O_3 NTs with GGO solution. The dispersion was then injected into a coagulation bath of 5 wt% $CaCl_2$–ethanol–water (1 : 3). Finally, the reduced fibers were obtained by thermal treatment at 400 °C under N_2 atmosphere for 4 h.

Fabrication of supercapacitors

Two fiber electrodes (~3 cm) were placed parallel to each other at an appropriate distance (~3 mm) on a pre-cleaned PET substrate. Two copper wires were connected at alternate opposite ends of the fibers by silver paste. Finally, the fibers were coated with the PVA : H_3PO_4 : H_2O (1 : 1 : 10) electrolyte to afford flexible all-solid-state fiber supercapacitors.

Acknowledgements

This work was supported by the National Natural Science Foundation of China (no. 21325417 and no. 51173162), the Huawei Innovation Research Program, the Fundamental Research Funds for the Central Universities (no. 2013XZZX003), and the Zhejiang Provincial Natural Science Foundation of China (no. R4110175).

Notes and references

1 K. T. Nam, D. W. Kim, P. J. Yoo, C. Y. Chiang, N. Meethong, P. T. Hammond, Y. M. Chiang and A. M. Belcher, *Science*, 2006, **312**, 885.
2 B. Scrosati, *Nat. Nanotechnol.*, 2007, **2**, 598.
3 H. Nishide and K. Oyaizu, *Science*, 2008, **319**, 737.
4 J. A. Rogers, T. Someya and Y. G. Huang, *Science*, 2010, **327**, 1603.
5 J. R. Miller and P. Simon, *Science*, 2008, **651**, 321.
6 P. Simon and Y. Gogotsi, *Nat. Mater.*, 2008, **7**, 845.
7 A. S. Arico, P. Bruce, B. Scrosati, J. M. Tarascon and W. Van Schalkwijk, *Nat. Mater.*, 2005, **4**, 366.
8 D. Pech, M. Brunet, H. Durou, P. H. Huang, V. Mochalin, Y. Gogotsi, P. L. Taberna and P. Simon, *Nat. Nanotechnol.*, 2010, **5**, 651.
9 L. L. Zhang and X. S. Zhao, *Chem. Soc. Rev.*, 2009, **38**, 2520.
10 G. Wang, L. Zhang and J. Zhang, *Chem. Soc. Rev.*, 2012, **41**, 797.
11 Y. P. Fu, X. Cai, H. W. Wu, Z. B. Lv, S. C. Hou, M. Peng, X. Yu and D. C. Zou, *Adv. Mater.*, 2012, **42**, 5713.
12 T. Chen, L. B. Qiu, Z. B. Yang, Z. B. Cai, J. Ren, H. P. Li, H. J. Lin, X. M. Sun and H. S. Peng, *Angew. Chem., Int. Ed.*, 2012, **51**, 11977.
13 J. Ren, L. Li, C. Chen, X. L. Chen, Z. B. Cai, L. B. Qiu, Y. G. Wang, X. R. Zhu and H. S. Peng, *Adv. Mater.*, 2013, **25**, 1155.
14 K. Wang, Q. H. Meng, Y. J. Zhang, Z. X. Wei and M. H. Miao, *Adv. Mater.*, 2013, **25**, 1494.
15 X. Li, T. Zhao, Q. Chen, P. Li, K. Wang, M. Zhong, J. Wei, D. Wu, B. Wei and H. Zhu, *Phys. Chem. Chem. Phys.*, 2013, **15**, 17752.
16 Z. Xu and C. Gao, *Nat. Commun.*, 2011, **2**, 571.
17 Z. Xu, Y. Zhang, P. G. Li and C. Gao, *ACS Nano*, 2012, **6**, 7103.
18 Z. L. Dong, C. C. Jiang, H. H. Cheng, Y. Zhao, G. Q. Shi, L. Jiang and L. T. Qu, *Adv. Mater.*, 2012, **24**, 1856.
19 Z. Xu, H. Y. Sun, X. L. Zhao and C. Gao, *Adv. Mater.*, 2013, **25**, 188.
20 T. Huang, B. Zheng, L. Kou, K. Gopalsamy, Z. Xu, C. Gao, Y. Meng and Z. Wei, *RSC Adv.*, 2013, **3**, 23957.
21 Y. R. Li, K. X. Sheng, W. J. Yuan and G. Q. Shi, *Chem. Commun.*, 2013, 291.
22 X. M. Li, T. S. Zhao, K. L. Wang, Y. Yang, J. Q. Wei, F. Y. Kang, D. H. Wu and H. W. Zhu, *Langmuir*, 2011, **27**, 12164.
23 Y. N. Meng, Y. Zhao, C. G. Hu, H. H. Cheng, Y. Hu, Z. P. Zhang, G. Q. Shi and L. T. Qu, *Adv. Mater.*, 2013, **25**, 2326.
24 Y. Huang, J. Liang and Y. Chen, *Small*, 2012, **8**, 1805.
25 E. Frackowiak, *Phys. Chem. Chem. Phys.*, 2007, **9**, 1774.
26 J. Bae, M. K. Song, Y. J. Park, J. M. Kim, M. Liu and Z. L. Wang, *Angew. Chem., Int. Ed.*, 2011, **50**, 1683.
27 L. Kou, T. Huang, B. Zheng, Y. Han, X. Zhao, K. Gopalsamy, H. Y. Sun and C. Gao, *Nat. Commun.*, 2014, **5**, 3754.
28 B. Zheng, T. Huang, L. Kou, X. Zhao, K. Gopalsamy and C. Gao, *J. Mater. Chem. A*, 2014, **2**, 9736.
29 X. Chen, S. Chen, W. Huang, J. Zheng and Z. Li, *Electrochim. Acta*, 2009, **54**, 7370.
30 A. P. Periasamy, S. Yang and S. Chen, *Talanta*, 2011, **87**, 15.
31 H. Wang, Z. Hu, Y. Chang, Y. Chen, Z. Lei, Z. Zhang and Y. Yang, *Electrochim. Acta*, 2010, **55**, 8974.
32 T. P. Gujar, V. R. Shinde, C. D. Lokhande and S. H. Han, *J. Power Sources*, 2006, **161**, 1479.

33 F. Zheng, G. Li, Y. Ou, Z. Wang, C. Su and Y. X. Tong, *Chem. Commun.*, 2010, **46**, 5021.
34 D. S. Yuan, J. H. Zeng, N. Kristian, Y. Wang and X. Wang, *Electrochem. Commun.*, 2009, **11**, 313.
35 Y. Li, J. Wang, Z. Deng, Y. Wu, X. Sun, D. Yu and P. Yang, *J. Am. Chem. Soc.*, 2001, **123**, 9904.
36 Z. Xu and C. Gao, *Acc. Chem. Res.*, 2014, **47**, 1267.
37 X. Hu, Z. Xu, Z. Liu and C. Gao, *Sci. Rep.*, 2013, **3**, 2374.

